Composites: Part A 161 (2022) 107110

Contents lists available at ScienceDirect

Composites Part A

journal homepage: www.elsevier.com/locate/compositesa

Impact and fatigue tolerant natural fibre reinforced thermoplastic composites by using non-dry fibres

F. Javanshour [a,*], A. Prapavesis [b], N. Pournoori [a], G.C. Soares [a], O. Orell [a], T. Pärnänen [a], M. Kanerva [a], A.W. Van Vuure [b], E. Sarlin [a]

[a] Unit of Materials Science and Environmental Engineering, Tampere University, Tampere, Finland
[b] Department of Materials Engineering, Composite Materials Group, KU Leuven, 3001 Leuven, Belgium

ARTICLE INFO

Keywords:
B. Adhesion
B. Debonding
B. Delamination
A. Thermoplastic matrix

ABSTRACT

This article introduces stiff and tough biocomposites with in-situ polymerisation of poly (methyl methacrylate) and ductile non-dry flax fibres. According to the results, composites processed with non-dry fibres (preconditioned at 50% RH) had comparable quasi-static in-plane shear strength but 42% higher elongation at failure and toughness than composites processed with oven-dried fibres. Interestingly, the perforation energy of flax–PMMA cross-ply composites subjected to low-velocity impact increased up to 100% with non-dry flax fibres. The in-situ impact damage progression on the rear surface of composites was evaluated based on strain and thermal field maps acquired by synchronised high-speed optical and thermal cameras. Impact-induced delamination lengths were investigated with tomography. Non-dry fibres also decreased the tension–tension fatigue life degradation rate of composites up to 21% and altered the brittle failure mode of flax–PMMA to ductile failure dominated by fibre pull-out.

1. Introduction

Natural flax fibre reinforced thermoplastic composites offer low density structural composites with good damping properties and recyclability [1–3]. Currently, the major application areas of continuous flax fibre reinforced composites are in the construction and sporting sectors [4]. The long-term durability of structural biocomposites is essential to promote the inherent ecological merit of natural fibres. The impact and fatigue tolerance of flax fibre composites are critical for their long-term durability [5–8]. The toughness of the reinforcing fibres and the polymer matrix [3,6,9], lay-up and architecture of the reinforcing fabrics [6], and interfacial toughness [10–12] are the critical parameters for composites' impact and fatigue tolerance. The primary failure mode of flax fibre composites is fibre failure with minor delamination, specifically in low-velocity impact incidents, limiting the energy dissipation potential [6,10]. Strong and tough interfacial adhesion can enhance stress transfer between fibre and matrix, deflect the interfacial cracks towards the matrix, and improve fatigue and impact tolerance [13]. The interfacial toughness of flax fibre composites should be designed to allow limited damage growth and further energy dissipation through interfacial debonding and delamination under low-velocity impact [10]. A tough interface can enhance the fatigue tolerance of composites [14,15]. Common methods to enhance interfacial toughness are chemical grafting of polymer chains on reinforcing fibres to induce polymer chain entanglement between fibre and matrix [16,17], depositing functionalised nanomaterials on the fibres [18–20], and deploying a thin ductile phase between fibre and matrix [10,13]. For instance, Hsieh et al. [15] showed that adding 0.5 wt% carbon nanotubes increases epoxy resin's fatigue crack growth threshold by 204% from 24 J/m^2 to 73 J/m^2. They reported a significant effect of nanotube debonding and pull-out on fracture toughness of epoxy, based on fractography observations and micromechanical modelling [15].

An alternative approach to enhance the toughness of natural fibre composites is to use non-dry (swollen) fibres and take advantage of the moisture present in the fibres [21–23]. The radial swelling coefficient of technical flax fibres ($\beta_{f,r}$: 1.9 [24]) is many orders of magnitude higher than their thermal expansion coefficient ($\alpha_{f,r}$:78 $\times$ 10^{-6}/°C [25]). In climates where the relative humidity is around 50% RH, processing biocomposites with fibres stored in the ambient condition (e.g., 23 °C, 50% RH) can be beneficial as the in-service swelling and shrinkage of fibres within composites will be limited compared to composites processed with oven-dried fibres [26,27]. Also, preserving the moisture of

* Corresponding author.
E-mail address: farzin.javanshour@tuni.fi (F. Javanshour).

https://doi.org/10.1016/j.compositesa.2022.107110
Received 24 May 2022; Received in revised form 15 July 2022; Accepted 20 July 2022
Available online 22 July 2022

flax fibres during the processing of composites can improve the ductility and tensile strength of reinforcing fibres and raise the impact and fatigue tolerance of composites [21,22,28].

In this study, non-dry flax fibre reinforced thermoplastic composites were manufactured through resin infusion by in-situ polymerisation of poly (methyl methacrylate) (PMMA). It was hypothesised that in-situ polymerisation of PMMA could be insensitive to water molecules as the MMA monomers are often emulsion polymerised in an aqueous medium [29]. Due to the reactive nature of in-situ polymerisation, good bonding between fibre and matrix was expected. The motivation to use non-dry fibres was to benefit from the enhancement in the ductility of flax fibres and to potentially raise interfacial toughness. Additionally, it was envisioned that the proposed processing method would save cost and energy by eliminating the need for oven-drying fibres, often required in manufacturing natural fibre composites [23,30].

The interfacial adhesion between fibre and matrix was evaluated based on quasi-static transverse tensile and in-plane shear testing of flax–PMMA composites. The fatigue and impact tolerance of cross-ply composites were assessed by applying low-cycle tension–tension fatigue and low-velocity drop-weight impact tests. After fatigue tests, the fracture surfaces of composites were investigated by scanning electron microscopy (SEM). The damage mechanism, deformation, and heat release on the rear surface of composites during impact testing were monitored with synchronised high-speed optical and infrared (IR) imaging. The internal through-thickness damage of impacted composite specimens was studied by X-ray computed tomography.

2. Methodology

Non-crimp flax yarn fabrics of unidirectional (UD) and twill 2/2 types with an areal density of 300 g/m^2 were provided by Bcomp (Fribourg, Switzerland). A thin polyester weft thread connected the yarns of the UD flax fabrics. The manufacturer treated the flax fibres with boiling water to remove waxes from the surface. The mechanical properties of these fibres are reported in Supplementary data (S.1.1). A liquid thermoplastic resin based on methyl methacrylate (Elium 188, Arkema, Colombes, France) and dibenzoyl peroxide initiator (BP-50-FT1, United Initiators GmbH, Pullach, Germany) with 3 wt% initiator to resin was used as the polymer matrix system. Elium 188 resin system was selected based on its excellent mechanical properties (see S.1.1) and the possibility of free radical polymerisation at ambient conditions [31,32]. Room temperature (23 °C) in-situ polymerisation of Elium 188 was selected to avoid evaporation of the moisture present in non-dry flax fibres. For simplicity, the resin system in this article (Elium 188) was named PMMA throughout the text.

In-situ polymerised flax–PMMA composite panels with a fibre volume fraction (V_f) of 40% were manufactured based on the vacuum-assisted resin infusion method (see Supplementary data, S.1.2). The V_f and composites' morphology were characterised by X-ray computed (X-CT) tomography (UniTom HR, TESCAN, Ghent, Belgium) with a voxel size of 800 nm as described in Supplementary data (S.1.3). Three types of composites (labelled as Dry, RT, and RH) were processed with flax fabrics stored in three different conditions for 24 h before resin infusion. Dry fabrics were oven-dried at 115 °C (for 24 h), RT fabrics were conditioned at 50% RH (23 °C, for 24 h), and RH fabrics were conditioned at 90% RH (23 °C, 24 h). The moisture content of fibres was measured by an analytical balance (model GR-202, A&D Ltd, Tokyo, Japan). The average weight for three pieces of fabrics (10 mm × 10 mm; width × length) was measured consecutively after oven-drying and humidity conditioning. The weight gains of RT and RH fabrics after conditioning were respectively 8.1 ± 0.2 wt% and 16.8 ± 0.2 wt% compared to oven-dried (Dry) fabrics. Laminates were then stored in a controlled environment (50% RH, 23 °C) for three months to reach equilibrium before testing. The weight gain values of Dry and RT composites at equilibrium were respectively 2.3 ± 0.1 wt% and 0.2 ± 0.1 wt %. The weight of RH-type composites was reduced by 4.1 ± 0.2 wt% upon reaching an equilibrium due to moisture desorption of swollen fibres. In this study, all relative humidity (RH) conditionings for both fabrics and composites were done in a humidity chamber (model VC 0018, Vötschtechnik, Balingen, Germany).

Quasi-static tensile testing was carried out with a universal testing machine (model 5967, Instron, MA, USA). The effect of non-dry fibres on interfacial adhesion was studied based on quasi-static transverse tensile strength of UD composites and in-plane shear testing of composites with $[+45/-45]_{SE}$ lay-ups according to ASTM D3039 and ASTM D3518 standards, respectively (for details see the Supplementary data S.1.4). The in-plane quasi-static properties were studied based on tensile testing of composites with $[(0,90)]_4$ lay-ups composed of four twill 2/2 woven fabric plies (ASTM D3039). Full-field deformation was measured with a stereo optical extensometer (StrainMaster Compact, LaVision, Göttingen, Germany). The specimen and test specifications are reported in Supplementary data (S.1.4). The average results of seven specimens per series (excluding grip failure) were reported.

The contribution of non-dry fibres to the fatigue resistance of flax–PMMA composites was evaluated by performing tension–tension cyclic tests of composites with $[(0,90)]_4$ lay-ups following the ASTM D3479 standard. Rectangular-shaped specimens were used with dimensions of 250 mm × 25 mm × 2 mm (length × width × thickness). Tapered glass-epoxy tabs were used to reduce the stress concentration at the gripped section of the specimens (as described in Supplementary data S.1.4). The tests were performed with a servo-hydraulic tester (MTS 180, Minnesota, USA) equipped with a 100 kN load cell and a gauge length of 150 mm. A constant-load amplitude and a sinusoidal wave shape were applied at a frequency of 5 Hz. The loading frequency of 5 Hz was chosen to avoid a temperature rise of more than 10 °C according to the ASTM D3479. The stress ratio (R) of the nominal minimum to maximum applied stress was 0.1. S-N graphs were acquired by registering the number of cycles to failure and the nominal maximum stress for each specimen. The load levels (90%, 80%, 70%, and 50%) for the low-cycle fatigue tests were selected as the ultimate tensile strength fractions. Three specimens per load level (excluding any grip failure) were tested. The temperature of the specimens during testing was monitored by a longwave IR camera (model Ti400, Fluke, Washington, USA) with thermal sensitivity of 0.05 °C at 30 °C. The ambient conditions during tests were 23 °C and 50% RH. The fracture surface analysis of composites was carried out with a ULTRAplus (Zeiss, Oberkochen, Germany) scanning electron microscope (SEM). A thin platinum-palladium (Pt-Pd) coating was used to ensure enough conductivity for the SEM samples.

The impact performance of structural flax–PMMA composites with a $[0/90]_{3SE}$ lay-up was studied with an instrumented drop-weight tester (Type 5, Rosand, Ohio, USA) without rebound impacts per ASTM D7136 and ASTM D5628 standards. Rectangular-shaped specimens with dimensions of 60 mm × 60 mm × 5 mm (length × width × thickness) were clamped between two steel fixtures with a circular test area (diameter 40 mm) representing a fixed support. The drop height was adjusted to 0.11, 0.22, 0.32, 0.44, 0.55, 0.66, 0.77, 0.88, 0.99, 1.11, 1.21, 1.32, 1.43, and 1.57 m to reach kinetic energies of 3, 6, 9, 12, 15, 18, 21, 24, 27, 30, 33, 36, 39, and 42 J, respectively; the mass of the impactor was 2772 g. A hemispherical steel-made head (diameter 12.7 mm) was fixed to the impactor. The contact force was measured using a load sensor (60 kN) between the head and the impactor structure. The force data were recorded at a 180 kHz frequency. The displacement of the impactor was numerically integrated from the measured contact force–time curve. For each impact energy level, three composite specimens were tested.

The rear surfaces of composites (opposite to the impacted surface) during the impact testing were in-situ monitored via mirrors placed under the specimens with a synchronised high-speed optical camera (Fastcam SA-X2, Photron, Tokyo, Japan) and high-speed IR camera (Fast IR-1500 M2K, Telops, Quebec City, Canada). A 50.8 by 50.8 mm unprotected gold mirror (PFSQ20-03-M03, THORLABS, Newton, United States) at 80 cm lens distance and a conventional mirror at 35 cm lens

distance were placed at an angle below the impact specimen to reflect the IR electromagnetic radiation and full-field deformations respectively. The emissivity of the composites in the infrared range (ability to emit infrared energy) was measured to convert radiometric temperature to surface temperature. Further information on the optical and infrared imaging methods and the DIC analysis is available in Supplementary data S.1.5. The impact-induced internal damage of composites was studied with X-ray computed (X-CT) tomography (UniTOM XL, TESCAN, Ghent, Belgium) with a voxel size of 35 μm (see Supplementary data S.1.3).

3. Results and discussions

3.1. Morphology analysis of composites based on X-CT tomography

The internal microstructures of flax–PMMA composites after three months of stabilisation at 50% RH (23 °C) are presented in Fig. 1. The Dry, RT and RH composites, which are respectively processed with oven-dried (at 115 °C) fibres and humidity-conditioned fibres at 50% RH (23 °C) and 90% RH (23 °C), all are nearly void-free within the matrix phase. The void-free structure of composites and moisture insensitivity of the PMMA resin is relevant to the synthesis type of methyl methacrylate, which is emulsion polymerisation in an aqueous medium [29]. However, the porosities in composites were mainly detected within flax yarns between the fibre and matrix region. The volume fraction of porosities was 0.2 ± 0.05% for Dry and RT composites, while the 4.33 ± 0.29% volume fraction of the RH-type composites was comprised of interfacial porosities. The fibre volume fractions of composites were 41.91 ± 1.92% (for Dry), 39.27 ± 1.72% (for RT), and 45.02 ± 3.05% (for RH). In Fig. 1, minimal traces of interfacial debonding between fibre and matrix are evident within fibre yarns in Dry composites (Fig. 1). The limited debonding lines (cracks) in Dry-type composite can be related to the swelling of oven-dried flax fibres during the stabilisation period at 50% RH. Debonding traces are visible in RT to a lesser extent, as fibres were stored in the 50% RH before and after manufacturing. On the contrary, highly swollen RH fibres have shrunk during the drying (stabilisation) period at 50% RH (Fig. 1). The extensive interfacial debonding lines (cracks) within fibre yarns are evident for RH-type composite. The average width of the cracks within fibre bundles (bundle splits) in RH is 9.7 ± 3.1 μm, which is 177% higher than the average width of bundle splits in Dry-type composite (3.5 ± 0.3 μm). The large debondings can dramatically reduce the interfacial shear strength of RH composites but enhance the damping potential of composites through interfacial sliding between fibre and matrix.

3.2. Quasi-static tensile properties of composites

Fig. 2 shows examples of the typical representative shear stress–strain curves of flax–PMMA composites with $[+45/-45]_{SE}$ lay-up. Also, a complete set of in-plane shear stress–strain curves are presented in the Supplementary data (Fig. S5). In this study, the τ_{12}^{offset} and τ_{12}^{max} respectively correspond to the stress values at 0.2% and 5% engineering shear strain according to the testing standard (ASTM D3518).

The in-plane shear performances of the Dry, RT and RH composites are summarised in Table 1. The shear chord modulus of elasticity (G_{12}^{chord}) for both Dry and RT composites is 1.6 ± 0.1 GPa showing that processing flax–PMMA composites with non-dry fibres does not have any adverse effect on the G_{12}^{chord}. A slightly lower mean value of G_{12}^{chord} for RH composites (−18.75%) compared to the reference Dry composites can be ascribed to the local interfacial porosities [33] due to the shrinkage of swollen RH fibres during the stabilisation period at 50% RH (23 °C). The mean τ_{12}^{offset} and τ_{12}^{max} values of RT composites are respectively 5.6% and 3.9% lower than Dry composites, which indicates comparable interfacial adhesion of flax–PMMA composites with both

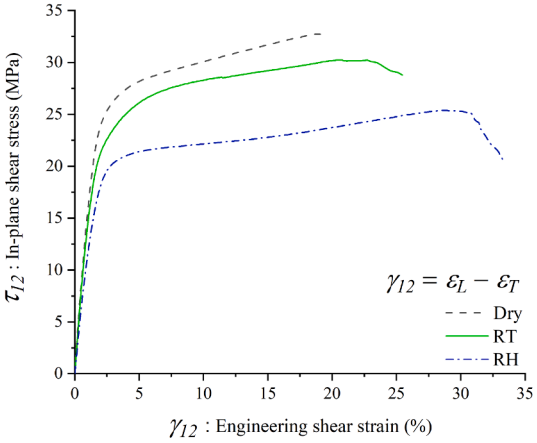

Fig. 2. The representative (average) in-plane shear stress–strain plots of flax–PMMA composites with $[+45/-45]_{SE}$ lay-up. (For interpretation of the references to colour in this figure legend, the reader is referred to the web version of this article.)

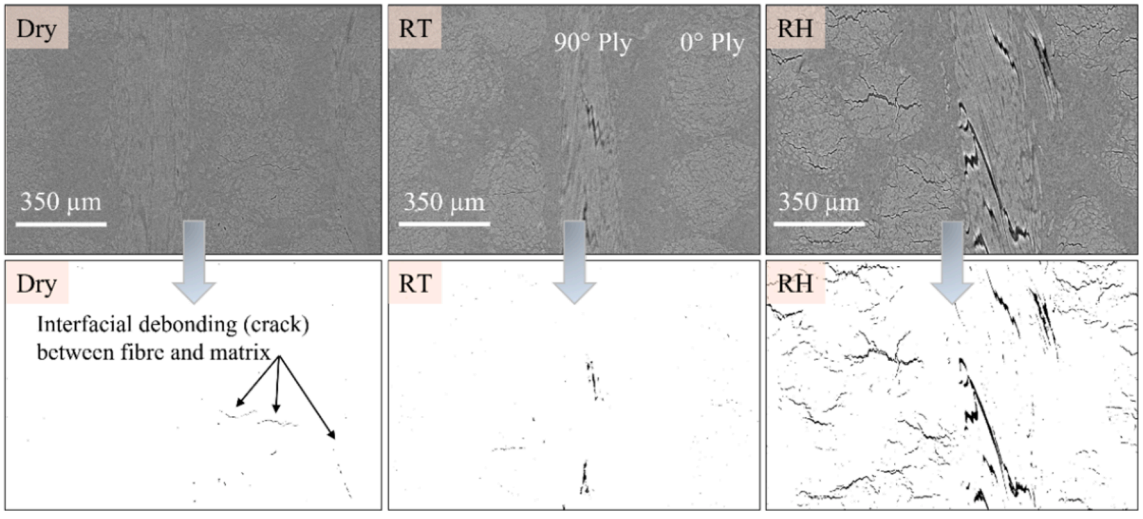

Fig. 1. X-CT tomography of flax–PMMA composites stabilised for three months at 50% RH (23 °C). (For interpretation of the references to colour in this figure legend, the reader is referred to the web version of this article.)

Table 1
In-plane shear properties of flax–PMMA composites with $[+45/-45]_{SE}$ lay-up.

Property	Dry Composites	RT Composites	RH Composites
G_{12}^{chord}, (GPa)	1.6 ± 0.1	1.6 ± 0.1	1.3 ± 0.1
τ_{12}^{offset}, (MPa)	17.6 ± 1.7	16.6 ± 1.4	13.1 ± 1.8
τ_{12}^{max}, (MPa)	27.7 ± 1.9	26.6 ± 1.3	21.3 ± 1.5
$\gamma_{12}{}^{failure}$, (%)	19.4 ± 1.2	27.6 ± 1.7	34.4 ± 1.9
Toughness, (MJ/m^3)	540.8 ± 8.1	768.2 ± 7.9	791.2 ± 9.9

oven-dried and non-dried (RT) fibres. However, the mean τ_{12}^{offset} and τ_{12}^{max} values of RH composites are 25.5% and 23.1% lower than of the Dry composites, which can be attributed to the lower adhesion between RH-flax fibre and PMMA and lower adhesion between elementary RH-flax fibres. Lower adhesion between fibre and matrix in RH composites is related to the extensive interfacial debonding sites due to fibre shrinkage, as discussed in the previous section through X-CT tomography analysis. The effect of humidity on technical flax fibres has been reported in the literature [22]. At humidity levels above 70% RH, the cementitious pectin layer on the elementary flax fibres binding fibres together within the technical fibres may soften by the water molecules [22]. The high humidity-induced softening can cause defibrillation of the technical flax fibres and reduce the strength of composites [23]. The mean elongation at failure values ($\gamma_{12}{}^{failure}$) of RT and RH composites are respectively 42.2% and 77.3% higher than for Dry composites. The tensile toughness values based on the area under stress–strain curves have a similar trend as the $\gamma_{12}{}^{failure}$. The significantly higher elongation at failure and tensile toughness of non-dry composites than the Dry specimens can be explained by the plasticising effect of moisture on the flax fibres [22] and modestly lower interfacial adhesion of RT and RH composites [10].

The quasi-static transverse tensile and in-plane tensile performance of the Dry, RT, and RH composites are provided in Table 2. Dry and RT composites have almost the same transverse tensile properties. The elastic modulus of PMMA (3.17 ± 0.2 GPa) dominates composites' transverse elastic (E_T) modulus. Similar E_T modulus values (3.1 GPa) of Dry and RT composites show that the in-situ polymerisation of flax–PMMA composites is not sensitive to the presence of moisture. The transverse elastic modulus and transverse tensile strength of RH composites are 48.4% and 38.6% lower than for the reference Dry composites. The extensive interfacial debonding sites caused by the shrinkage of swollen fibres (at 90% RH) are the reason for the degradation in the transverse tensile strength and E_T of RH composites. The quasi-static tensile performance of composites (in Table 2) with $[(0,90)]_4$ lay-up follows the same trend as in transverse tensile and in-plane shear. The quasi-static results showed that the in-situ polymerisation of flax–PMMA composites is not sensitive to ambient moisture. In summary, non-dry composites offered a unique combination of ductility and good in-plane shear strength, beneficial characteristics for fatigue and impact tolerant structural biocomposites.

3.3. Fatigue performance of composites

Fig. 3(A) demonstrates the tension–tension fatigue performance of flax–PMMA composites. The fatigue behaviour of Dry, RT and RH composites follows a similar trend in the various loading ranges. The S-N slope of RH (−12.45) is less steep compared to Dry (−15.87), which indicates a 21% longer fatigue life for RH composites that have a more significant elongation at failure (see Table 2). For instance, at the 80% load level, the number of cycles to failure of RH composites is 80% higher than Dry-type composites. The S-N slope of Dry and RT composites are similar. As shown in Fig. 3(B), processing composites with non-dry fibres alters the brittle fatigue failure mode of Dry flax–PMMA composites into a more ductile failure dominated by the fibre pull-out which enhances the energy dissipation and fatigue tolerance of composites due to interfacial sliding [34]. Figs. 4 and 5 provide further insights into the fatigue failure mode of composites.

Fig. 4(A) presents a general view of the tension–tension fatigue fracture surface of the Dry composites with ply divisions. Fig. 4(B and C) suggest overall good adhesion between fibre and matrix and brittle fibre failure in Dry-type flax–PMMA composites with some extent of fibre pull-out and fibre imprints. Fig. 4(D) demonstrates regular wave-like features commonly known as striations. The striations form due to the molecular chain fracture at the crack tip following limited stretching [35]. The striations on the fracture surface show the incremental nature of damage growth following the loading cycles [35].

In Fig. 5(A, B), the fatigue fracture surfaces of RT composite resemble those of Dry specimens (Fig. 4A, B) except for a more considerable extent of fibre pull-out. The polymer residues on the fibre surfaces of RT composites indicate good compatibility between fibre and matrix (Fig. 5B). The fracture surface of the RH composite in Fig. 5(C, D) is dominated by extensive and lengthy fibre pull-outs with smooth fibre surfaces. The fractographic results in this section confirm the ductile nature and higher fatigue energy dissipation capability of non-dry composites by interfacial fibre-sliding compared to Dry composites.

Table 2
Quasi-static tensile properties of the flax–PMMA composites. The $[90]_4$ and $[(0,90)]_4$ lay-ups are respectively composed of four UD and twill-woven fabric layers.

Composite, Lay-up	E^{chord}, (GPa)	σ^{max}, (MPa)	$\varepsilon^{failure}$, (%)
Dry, $[90]_4$	3.1 ± 0.3	14.5 ± 0.3	0.41 ± 0.05
RT, $[90]_4$	3.1 ± 0.2	13.7 ± 0.7	0.42 ± 0.02
RH, $[90]_4$	1.6 ± 0.1	8.9 ± 0.6	0.72 ± 0.01
Dry, $[(0,90)]_4$	11.7 ± 0.2	110.2 ± 1.8	1.62 ± 0.06
RT, $[(0,90)]_4$	11.4 ± 0.1	105.2 ± 1.2	1.83 ± 0.05
RH, $[(0,90)]_4$	8.4 ± 0.1	94.5 ± 1.4	2.44 ± 0.08

3.4. Drop-weight impact performance

Composites can absorb part of the impact energy by plastic deformation and transfer the remaining elastic part of the energy back to the impactor, depending on their impact resistance and elasticity. The perforation energy (E^P) is a characteristic where the specimen fails without recovered elastic energy. Fig. 6 (A) provides an overview of the drop-weight impact energy-time history of cross-ply flax–PMMA composites with a $[0/90]_{3SE}$ lay-up. The energy-time curves show that processing flax–PMMA composites with non-dry fibres enhances the E^P of the reference Dry composites (21 J) by 57% (RT: 33 J) and 100% (RH: 42 J). Fig. 6 (B) summarises the E^P values of composites normalised to the thickness of the specimens. It is worth noting that the 21 J (4.06 ± 0.13 J/mm) perforation energy (E^P) of the Dry flax–PMMA composites in this study is equal to the E^P of flax/epoxy composites with a similar reinforcement type and lay-up ($[0/90]_{3SE}$ lay-up, 5 mm in thickness, 40% V_f) [10]. Compared to the flax fibre reinforced poly (lactic acid) (PLA) composites, the E^P of the Dry flax–PMMA composites (21 J, 4.06 ± 0.13 J/mm) is 16% higher than flax/PLA composites (E^P = 3.49 ± 0.41 J/mm) made of 2 × 2 twill flax/PLA commingled textile with $[(0/90)]_{12}$ lay-up, 4 mm in thickness and 32% V_f [36]. Also, processing flax fibre reinforced composites with thermoplastic matrix systems, which are more ductile compared to PMMA, can result in better E^P values for biocomposites. For instance, flax fibre reinforced polypropylene (PP) composites with $[(0,90)]_{10}$ lay-up made of 2 × 2 twill flax/PP commingled textile, 40% V_f, and 3 mm in thickness have the perforation energy of 15 J (or 5 J/mm) [37] which is 23% higher than the E^P value for Dry-type flax–PMMA (4.06 ± 0.13 J/mm). However, the non-dry RT and RH composites reported in this study offer the highest perforation energy for natural fibre composites in the literature with a unique combination of stiffness, toughness, and fatigue tolerance.

Fig. 7 shows the internal damage patterns of cross-ply specimens after 21 J impact testing. Contrary to the fully perforated Dry specimen, the damage patterns of the RT specimen are shear-induced ply splitting

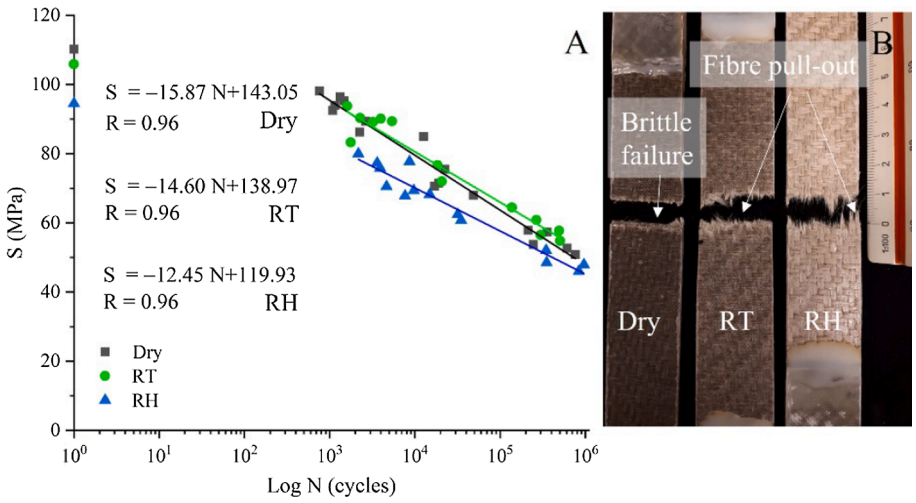

Fig. 3. Determined S-N curves of composites (A) and examples of the typical specimen failure modes (B). (For interpretation of the references to colour in this figure legend, the reader is referred to the web version of this article.)

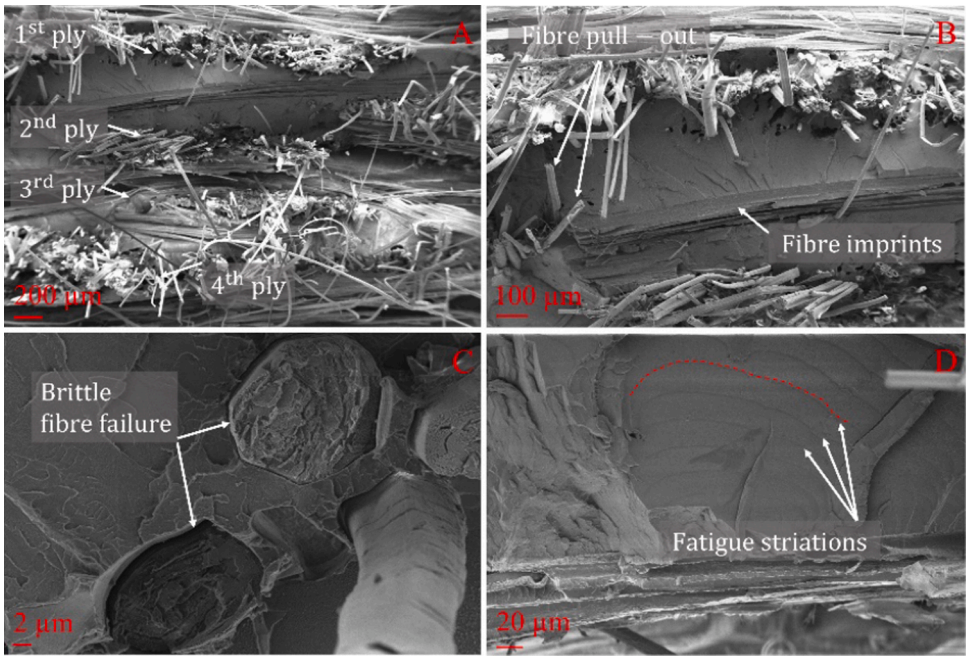

Fig. 4. The tension–tension fatigue fracture surface of Dry composites (A, B, C, D). (For interpretation of the references to colour in this figure legend, the reader is referred to the web version of this article.)

and five clear delamination lines with a cumulative length of 112.56 mm. The internal damage patterns of the RH specimen are local interfacial debonding and four clear delamination lines with a cumulative length of 82.05 mm, which is 27% lower than the corresponding value for RT (112.56 mm). The RH's lower extent of delamination and fibre failure agrees with RH's higher recovered impact energy than for RT at 21 J impact energy (see Fig. 6A). The X-CT results reflect the tough nature of non-dry composites, which allows dissipation of impact energy through interfacial sliding/debonding and delamination.

Fig. 8 shows the contact force–time history of composites at 21 J impact energy. Overall, the contact force–time profiles of the RT and RH composites are smoother and more symmetric compared to the profile for the Dry specimens, which indicates a higher degree of elastic deformation for non-dry specimens during the impact testing. Further data on full-field deformation of the specimen's rear surface is provided (in Figs. 9 and 10) for a better understanding of the impact damage mechanisms of flax– PMMA composites at perforation energy and the contribution of non-dry fibres. The full-field strain maps in Figs. 9 and 10 are synchronised with the contact force–time profiles (Fig. 8) to provide insights into specific force values.

The impact damage initiation and progression on the rear surface of the Dry specimen at 21 J impact energy is presented in Fig. 9 based on the in-situ high-speed optical and thermal-field imaging. The A–H images in Fig. 9 correspond to the specified force–time values (I–VII) in Fig. 8(A). For better visualisation of the 2D damage initiation and progression on the rear surface of the specimen, the von Mises strain maps are superimposed on the high-speed optical images in Fig. 9(A–D). However, the strain maps are removed after the crack opening on the rear surface of the specimen (Fig. 9E–G) due to the strain field discontinuity, especially in the vicinity of the crack.

In Fig. 9(A and B), the impact damage on the rear surface of Dry composite initiates as matrix cracking and develops further with ply

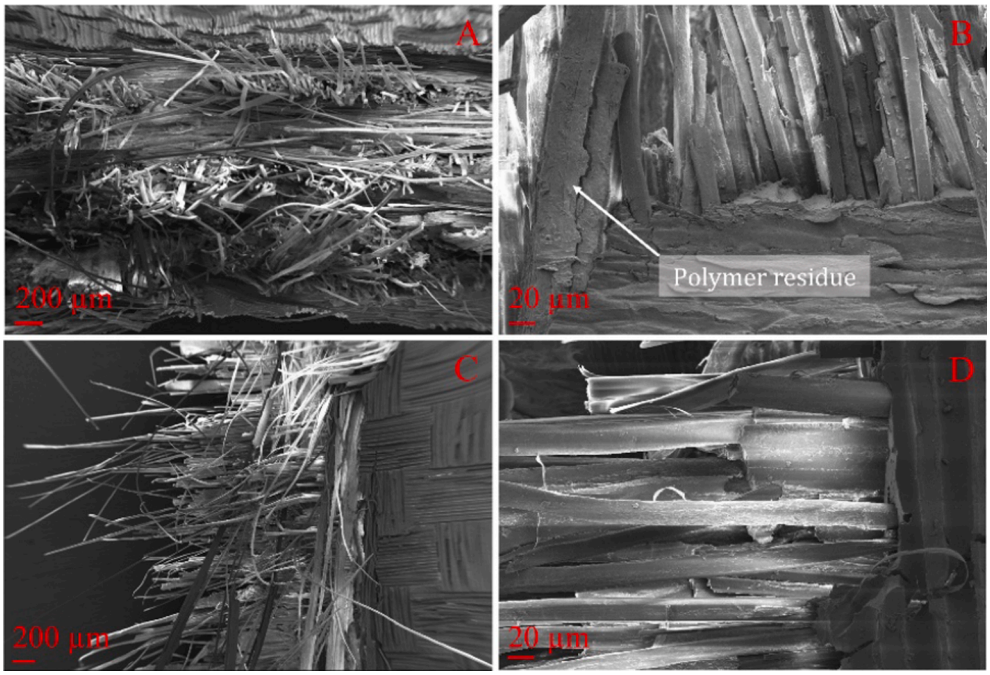

Fig. 5. The tension–tension fatigue fracture surface of RT (A, B) and RH (C, D) composites. (For interpretation of the references to colour in this figure legend, the reader is referred to the web version of this article.)

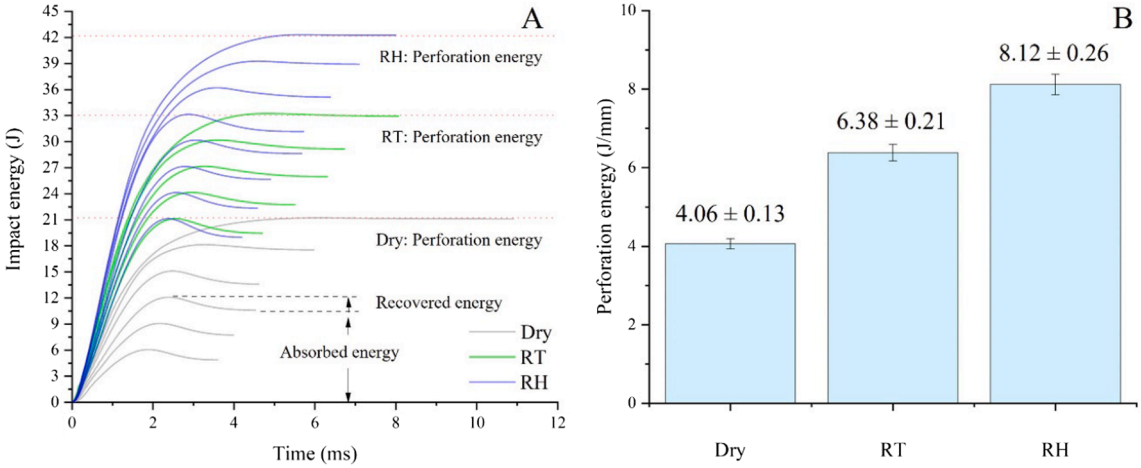

Fig. 6. Energy-time history of composites (A) and perforation energies normalised to thickness (B). (For interpretation of the references to colour in this figure legend, the reader is referred to the web version of this article.)

splitting (i.e., cracks between fibres) traces. The first crack opening (Fig. 9C) occurs at the maximum contact force (F^{max}). The crack propagates parallel to the fibre direction on the rear surface of the composite (Fig. 9D), which corresponds to the plateau region between the force values of III and IV in the contact force–time profile in Fig. 8(A). Fig. 8 (A) shows that the contact force continuously decreases after the plateau region (III-IV) until complete perforation. After the plateau region, the first drop in the contact force follows the development of extensive ply splitting and fibre pull-outs on the rear surface of the specimen (Fig. 9E and F). Transverse cracks develop just before the complete perforation (point VII in Fig. 8A), as shown in Fig. 9(G). The shape of surface cracks is visible in the thermal field image (Fig. 9H), which shows how the specimen dissipates the mechanical energy by heat generation.

To compare the Dry, RT, and RH composites, the von Mises strain maps at the maximum contact force (F^{max}) are presented in Fig. 10. In all cases, the crack opening happens at the F^{max}. The extent of the surface deformations is notably higher in RT and RH composites than in the Dry specimen. The strain maps at F^{max} show that the RT and RH composites have better ductility under impact loading than the Dry specimen.

The contact force-central displacement traces of composites at 21 J kinetic energy are presented in Fig. 11(A). Compared to Dry, the force–displacement curves of RT and RH composites are smoother and more symmetric, showing that the non-dry composites have a higher degree of elastic behaviour. In Fig. 11 (B), the maximum contact force (F^{max}) of the RT and RH composites at 21 J kinetic energy are respectively 13% and 19% above the similar value for the Dry specimens. The higher F^{max} values for RT and RH compared to the Dry specimens can be explained by the limited degree of the fibre and ply failure within non-dry composites at 21 J kinetic energy (as shown previously in Fig. 7), which enhances the load-bearing capacity of RT and RH. It is worth noting that the F^{max} of the Dry flax–PMMA composites in this study is in the same range as the F^{max} of flax/epoxy composites (4.209 ± 0.08 kN)

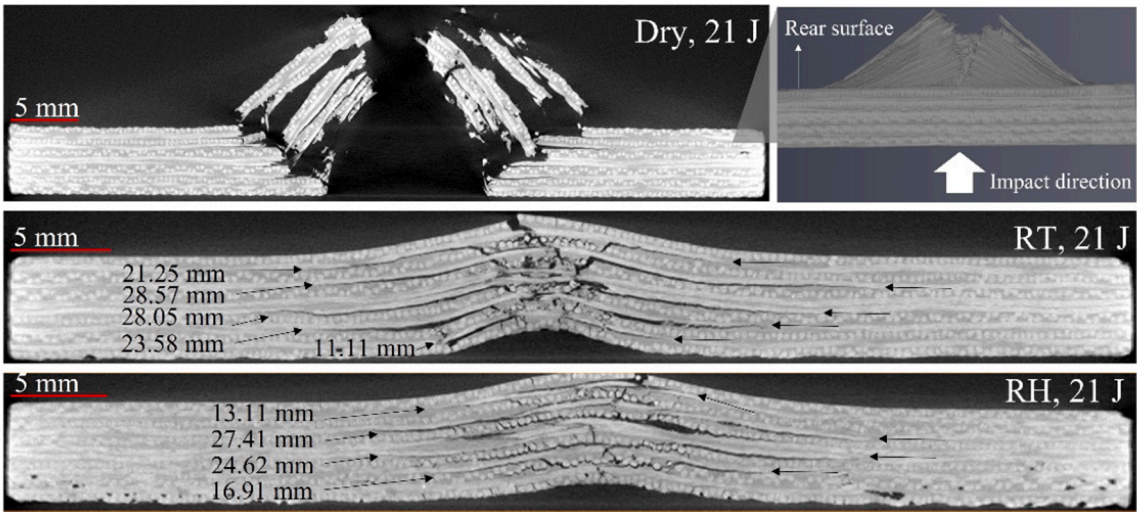

Fig. 7. Non-destructively captured internal damage patterns, including delamination lengths based on X-CT. (For interpretation of the references to colour in this figure legend, the reader is referred to the web version of this article.)

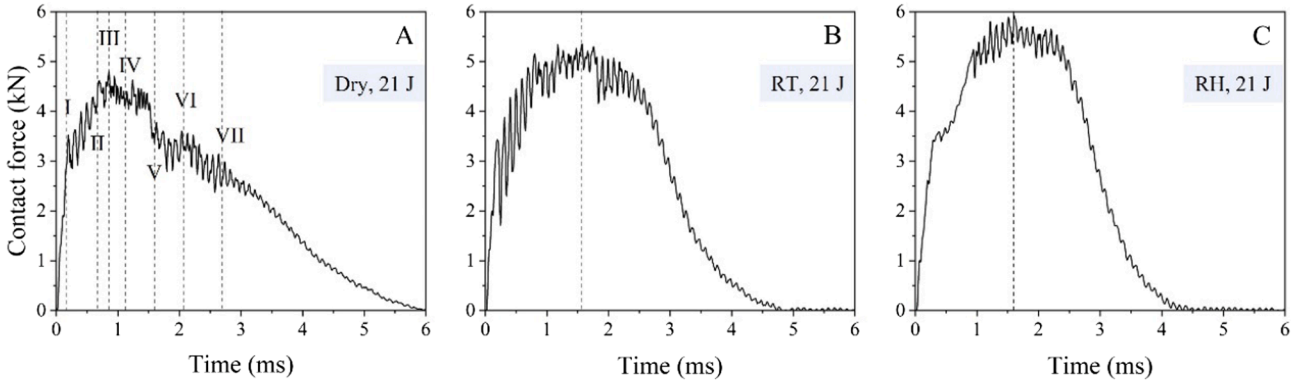

Fig. 8. Typical contact force–time history of composites at 21 J drop-weight impact energy. (For interpretation of the references to colour in this figure legend, the reader is referred to the web version of this article.)

with $[0/90]_{3SE}$ lay-up, 40% V_f, and 5 mm in thickness [10].

In Fig. 11(C), the average displacement values at F^{max} for RT and RH are respectively 45% and 61% higher than those values for Dry. The higher displacement values in Fig. 11 (C) for RT and RH compared to the Dry agree with the strain values reported in Fig. 10 and prove that the non-dry specimens present more ductile resistance against the impactor. Further data on contact force-central displacement traces of composites at various kinetic energies are available in the Supplementary data (Figs. S6–S8).

Fig. 12 shows the synchronised profiles of the contact force–time and temperature on the rear surface of composites at 21 J impact energy. In all composites, the average surface temperature rises only after the first peak in the contact force–time history, which corresponds to the initiation of matrix cracks and ply splitting on the rear surface of the composites. So, the increase in the surface temperature of specimens is directly related to and proportional to the plastic deformations during the impact incident. Therefore, it can be concluded that the extent of plastic deformations is the highest for the Dry specimen, while RT and RH specimens present more elastic resistance against the impactor. It is worth noting that the increase in the average surface temperature of natural fibre composites (for both perforated and non-perforated specimens) is less than 5 °C (Fig. 12). However, low-velocity impact is not an adiabatic process, and specimens have sufficient time to dissipate the mechanical energy as heat [38]. The specimens have sufficient time to dissipate low-velocity impact energy as heat to a large volume before reaching the rear surface, where an IR camera collects temperature maps. So, the initial temperature rise inside the specimens might be higher than at the rear surface as the damage propagates through the thickness. Additional studies are necessary to understand further the effect of impact-induced heat release on the material behaviour of composites.

4. Summary and outlook

In summary, non-dry fibres modified the brittle nature of flax–PMMA composites through toughening due to the plasticising effect of moisture bound to fibres [22] and interfacial toughening by allowing interfacial sliding. Especially, RT composites with preconditioned fibres (stored in 50% RH, 23 °C for 24 h) can positively impact further use of environmentally friendly natural fibres in structural applications. RT offered good adhesion between fibre and matrix, same as oven-dried fibres, higher in-plane shear strain (42%), lower fatigue life degradation, and 57% higher perforation energy than commonly used oven-dried flax fibre composites. These results are valuable as designing stiff and tough composites with simultaneous fatigue and impact tolerance enhancement can be challenging. The polymerisation kinetic studies in the literature [32,39] suggest the possibility of processing thick composite laminates in the range of 10–20 mm without reaching 100 °C (at ambient pressure) to avoid boiling MMA monomers and the moisture present in the fibres. However, further research is required to

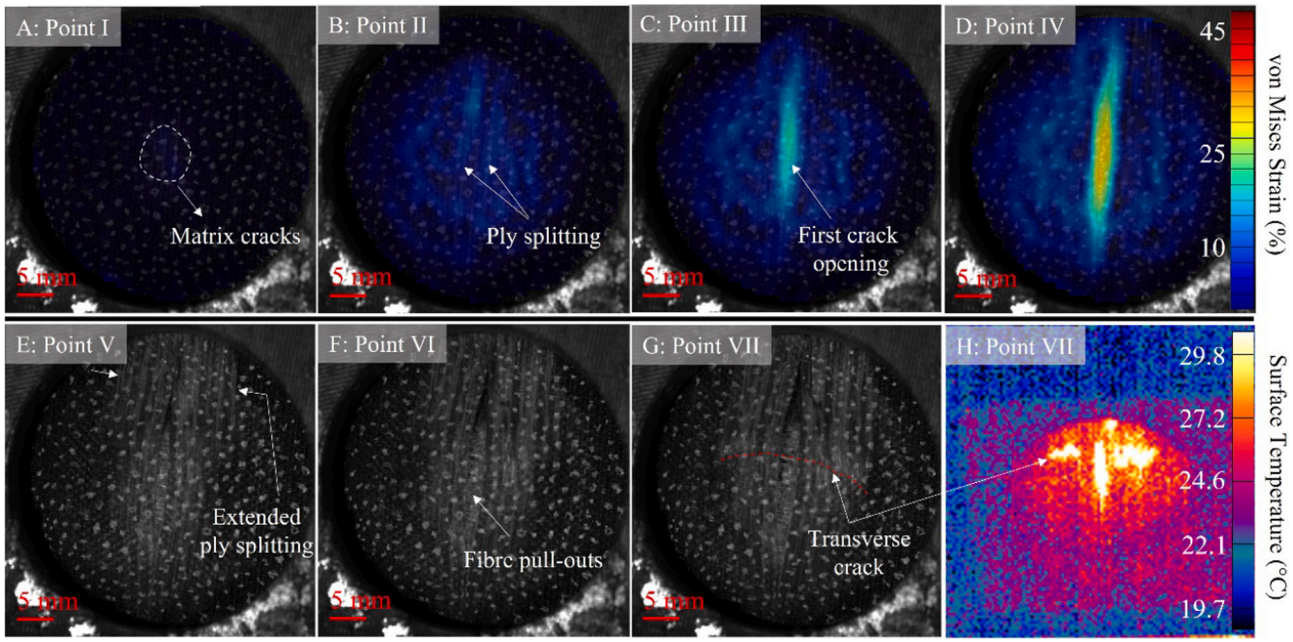

Fig. 9. Damage progression on the rear surface of Dry composite at 21 J impact energy. Figures A-H correspond to the specified force values (I-VII points in Fig. 8) in the force–time history of Dry composites. (For interpretation of the references to colour in this figure legend, the reader is referred to the web version of this article.)

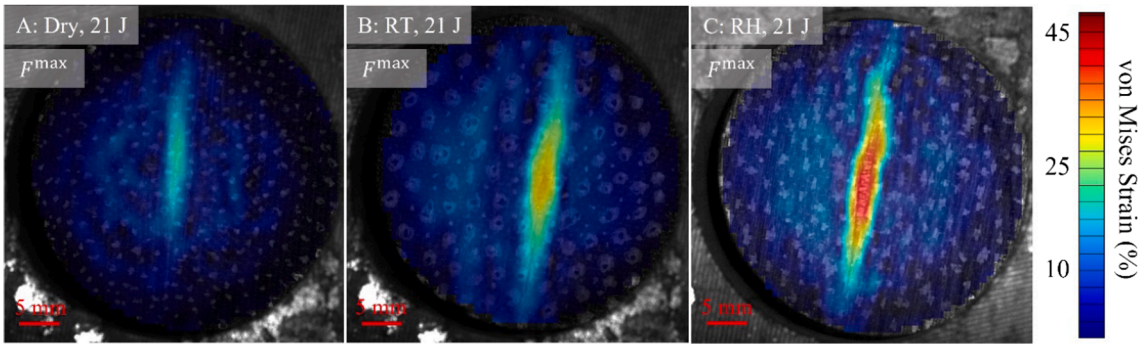

Fig. 10. Damage patterns on the rear surface of Dry (A), RT (B), and RH (C) composites at 21 J impact energy. (For interpretation of the references to colour in this figure legend, the reader is referred to the web version of this article.)

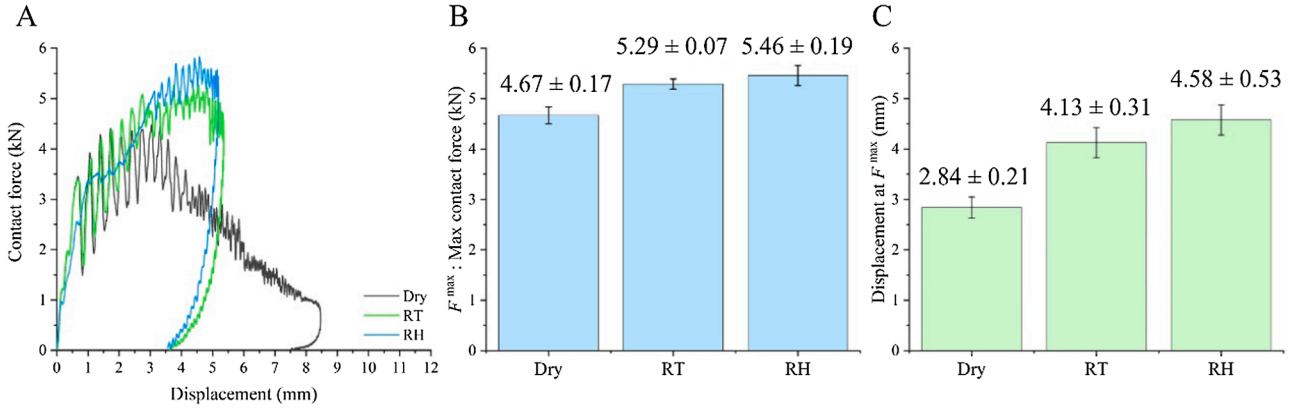

Fig. 11. Typical contact force-central displacement traces of the flax–PMMA composites after drop-weight impact testing at 21 J kinetic energy (A). The maximum contact force (F^{max}) and the corresponding displacement at F^{max} at 21 J kinetic energy are respectively presented in (B) and (C). (For interpretation of the references to colour in this figure legend, the reader is referred to the web version of this article.)

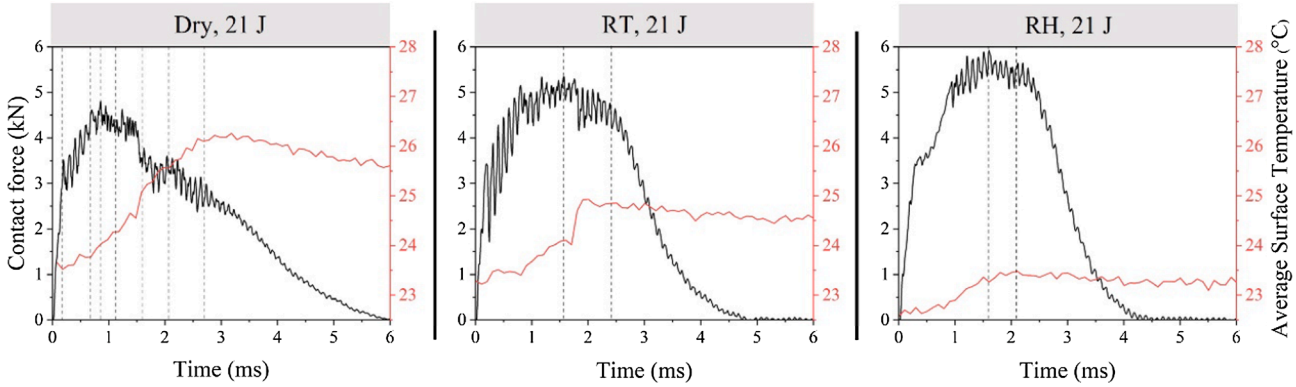

Fig. 12. Contact force–time and corresponding surface temperature–time history of composites at 21 J drop-weight impact energy. (For interpretation of the references to colour in this figure legend, the reader is referred to the web version of this article.)

understand the viability of processing in-situ polymerised non-dry natural fibre–PMMA composites with complex geometries of variable thicknesses [32]. It should be noted that the results in this article are valid only for composites equilibrated at the 50% RH (23 °C). In future work, the hygrothermal fatigue performance of flax–PMMA will have to be analysed to understand the effect of non-dry fibres on the long-term durability and dimensional stability of composites.

5. Conclusions

This paper proved the feasibility of processing stiff and tough structural flax–PMMA composites with non-dry fibres, which are relatively ductile compared to commonly used oven-dried fibres. The results presented in this article are valid mainly for indoor applications and composites equilibrated at 50% RH (23 °C). Composites with oven-dried and preconditioned (50% RH, 23 °C for 24 h) fibres had similar tensile moduli, transverse tensile strength, and in-plane shear strength. Preconditioning fibres in 90% RH decreased the transverse tensile strength (−38%) and in-plane shear strength (−23%) of composites because of the interfacial debonding sites due to the fibre shrinkage and plasticising effect of moisture on the fibres. Non-dry fibres preconditioned at 50% RH (RT), and 90% RH (RH) respectively enhanced the in-plane shear strain to failure of flax–PMMA (Dry) by 42% and 77%. Non-dry composites had a lower fatigue life degradation rate than oven-dried flax–PMMA composites. The fracture surface analysis manifested the better fatigue life and damage tolerance of non-dry composites as the result of ductile failure with extensive fibre pull-outs. In low-velocity drop-weight impact testing of cross-ply specimens, modified composites (RT and RH) had overall better elasticity against the impact loading, limited fibre failure and higher energy dissipation through extensive fibre pull-out and delamination compared to unmodified (Dry) material. RT and RH composites, respectively, raised the perforation energy of Dry by 57% and 100%. The synchronised strain and contact force data effectively could be linked to in-situ impact damage progression on the rear surface of composites. The DIC and IR data were coherent and complementary to the internal impact damage patterns acquired by X-CT.

CRediT authorship contribution statement

F. Javanshour: Conceptualization, Methodology, Formal analysis, Investigation, Writing – original draft, Visualization. **A. Prapavesis:** Investigation, Formal analysis, Writing – review & editing. **N. Pournoori:** Investigation, Formal analysis, Writing – review & editing. **G.C. Soares:** Investigation, Formal analysis, Writing – review & editing. **O. Orell:** Investigation, Formal analysis, Writing – review & editing. **T. Pärnänen:** Formal analysis. **M. Kanerva:** Funding acquisition, Writing – review & editing. **A.W. Van Vuure:** Funding acquisition, Writing – review & editing. **E. Sarlin:** Supervision, Investigation, Funding acquisition, Writing – review & editing.

Declaration of Competing Interest

The authors declare that they have no known competing financial interests or personal relationships that could have appeared to influence the work reported in this paper.

Data availability

Data will be made available on request.

Acknowledgements

This project is funded by the European Union's Horizon 2020 research and innovation programme under the Marie Skłodowska-Curie grant agreement No 764713-FibreNet. This work made use of Tampere Microscopy Center facilities at Tampere University. The authors thank Bcomp (Fribourg, Switzerland) for supplying the flax fabrics. Farzin Javanshour appreciates the contributions made by Apolline Féré (for fatigue testing) and Quynh Nguyen (for processing of composites).

Appendix A. Supplementary material

Supplementary data to this article can be found online at https://doi.org/10.1016/j.compositesa.2022.107110.

References

[1] Awais H, Nawab Y, Amjad A, Anjang A, Md Akil H, Zainol Abidin MS. Environmental benign natural fibre reinforced thermoplastic composites: a review. Compos Part C Open Access 2021;4:100082. https://doi.org/10.1016/J.JCOMC.2020.100082.

[2] Rueppel M, Rion J, Dransfeld C, Fischer C, Masania K. Damping of carbon fibre and flax fibre angle-ply composite laminates. Compos Sci Technol 2017;146:1–9. https://doi.org/10.1016/J.COMPSCITECH.2017.04.011.

[3] Woigk W, Fuentes CA, Rion J, Hegemann D, van Vuure AW, Kramer E, et al. Fabrication of flax fibre-reinforced cellulose propionate thermoplastic composites. Compos Sci Technol 2019;183:107791.

[4] Pil L, Bensadoun F, Pariset J, Verpoest I. Why are designers fascinated by flax and hemp fibre composites? Compos Part A Appl Sci Manuf 2016;83:193–205. https://doi.org/10.1016/J.COMPOSITESA.2015.11.004.

[5] Panciroli R, Giannini O. Comparing the impact resistance of flax/epoxy and glass/epoxy composites through experiments and numerical simulations. Compos Struct 2021;264:113750. https://doi.org/10.1016/J.COMPSTRUCT.2021.113750.

[6] Bensadoun F, Depuydt D, Baets J, Verpoest I, van Vuure AW. Low velocity impact properties of flax composites. Compos Struct 2017;176:933–44. https://doi.org/10.1016/j.compstruct.2017.05.005.

[7] Mahboob Z, Bougherara H. Fatigue of flax-epoxy and other plant fibre composites: Critical review and analysis. Compos Part A Appl Sci Manuf 2018;109:440–62. https://doi.org/10.1016/J.COMPOSITESA.2018.03.034.

[8] Mahboob Z, Fawaz Z, Bougherara H. Fatigue behaviour and damage mechanisms under strain controlled cycling: comparison of Flax–epoxy and Glass–epoxy composites. Compos Part A Appl Sci Manuf 2022;159:107008. https://doi.org/10.1016/J.COMPOSITESA.2022.107008.
[9] Van Vuure AW, Vanderbeke J, Mosleh Y, Verpoest I, El-Asmar N. Ductile woven silk fibre thermoplastic composites with quasi-isotropic strength. Compos Part A Appl Sci Manuf 2021;147:106442. https://doi.org/10.1016/J.COMPOSITESA.2021.106442.
[10] Javanshour F, Prapavesis A, Pärnänen T, Orell O, Lessa Belone MC, Layek RK, et al. Modulating impact resistance of flax epoxy composites with thermoplastic interfacial toughening. Compos Part A Appl Sci Manuf 2021;150:106628.
[11] Woigk W, Fuentes CA, Rion J, Hegemann D, van Vuure AW, Dransfeld C, et al. Interface properties and their effect on the mechanical performance of flax fibre thermoplastic composites. Compos Part A Appl Sci Manuf 2019;122:8–17.
[12] Randall JD, Stojcevski F, Djordjevic N, Hendlmeier A, Dharmasiri B, Stanfield MK, et al. Carbon fiber polypropylene interphase modification as a route to improved toughness. Compos Part A Appl Sci Manuf 2022;159:107001.
[13] Lin J, Wang L, Liu L, Lu K, Li G, Yang X. Two-stage interface enhancement of aramid fiber composites: establishment of hierarchical interphase with waterborne polyurethane sizing and oxazolidone-containing epoxy matrix. Compos Sci Technol 2020;193:108114. https://doi.org/10.1016/j.compscitech.2020.108114.
[14] AhmadvashAghbash S, Breite C, Mehdikhani M, Swolfs Y. Longitudinal debonding in unidirectional fibre-reinforced composites: Numerical analysis of the effect of interfacial properties. Compos Sci Technol 2022;218:109117. https://doi.org/10.1016/J.COMPSCITECH.2021.109117.
[15] Hsieh TH, Kinloch AJ, Taylor AC, Kinloch IA. The effect of carbon nanotubes on the fracture toughness and fatigue performance of a thermosetting epoxy polym. J Mater Sci 2011;46:7525–35. https://doi.org/10.1007/S10853-011-5724-0/FIGURES/9.
[16] Eyckens DJ, Demir B, Randall JD, Gengenbach TR, Servinis L, Walsh TR, et al. Using molecular entanglement as a strategy to enhance carbon fiber-epoxy composite interfaces. Compos Sci Technol 2020;196:108225.
[17] Randall JD, Eyckens DJ, Sarlin E, Palola S, Andersson GG, Yin Y, et al. Mixed surface chemistry on carbon fibers to promote adhesion in epoxy and PMMA polymers. Ind Eng Chem Res 2022;61:1615–23. https://doi.org/10.1021/ACS.IECR.1C04409/ASSET/IMAGES/LARGE/IE1C04409_0008.JPEG.
[18] Javanshour F, Ramakrishnan KR, Layek RK, Laurikainen P, Prapavesis A, Kanerva M, et al. Effect of graphene oxide surface treatment on the interfacial adhesion and the tensile performance of flax epoxy composites. Compos A Appl Sci Manuf 2021;142:106270.
[19] Kanerva M, Korkiakoski S, Lahtonen K, Jokinen J, Sarlin E, Palola S, et al. DLC-treated aramid-fibre composites: tailoring nanoscale-coating for macroscale performance. Compos Sci Technol 2019;171:62–9.
[20] Palola S, Javanshour F, Azari SK, Koutsos V, Sarlin E. One Surface Treatment, Multiple possibilities: broadening the use-potential of para-aramid fibers with mechanical adhesion. Polym 2021;13:3114. https://doi.org/10.3390/POLYM13183114.
[21] Berges M, Léger R, Placet V, Person V, Corn S, Gabrion X, et al. Influence of moisture uptake on the static, cyclic and dynamic behaviour of unidirectional flax fibre-reinforced epoxy laminates. Compos Part A Appl Sci Manuf 2016;88:165–77.
[22] Thuault A, Eve S, Blond D, Bréard J, Gomina M. Effects of the hygrothermal environment on the mechanical properties of flax fibres: Http://DxDoiOrg/101177/0021998313490217 2013;48:1699–707. https://doi.org/10.1177/0021998313490217.
[23] Fuentes CA, Ting KW, Dupont-Gillain C, Steensma M, Talma AG, Zuijderduin R, et al. Effect of humidity during manufacturing on the interfacial strength of non-pre-dried flax fibre/unsaturated polyester composites. Compos Part A Appl Sci Manuf 2016;84:209–15.
[24] Lu MM, Fuentes CA, Van Vuure AW. Moisture sorption and swelling of flax fibre and flax fibre composites. Compos Part B Eng 2022;231:109538. https://doi.org/10.1016/J.COMPOSITESB.2021.109538.
[25] le Duigou A, Merotte J, Bourmaud A, Davies P, Belhouli K, Baley C. Hygroscopic expansion: A key point to describe natural fibre/polymer matrix interface bond strength. Compos Sci Technol 2017;151:228–33. https://doi.org/10.1016/J.COMPSCITECH.2017.08.028.
[26] Lu MM, Van Vuure AW. Improving moisture durability of flax fibre composites by using non-dry fibres. Compos Part A Appl Sci Manuf 2019;123:301–9. https://doi.org/10.1016/J.COMPOSITESA.2019.05.029.
[27] Newman RH. Auto-accelerative water damage in an epoxy composite reinforced with plain-weave flax fabric. Compos Part A Appl Sci Manuf 2009;40:1615–20. https://doi.org/10.1016/J.COMPOSITESA.2009.07.010.
[28] Ahmad F, Abbassi F, Ul-Islam M, Jacquemin F, Hong JW. Enhanced impact-resistance of aeronautical quasi-isotropic composite plates through diffused water molecules in epoxy. Sci Rep 2021.1–13.;2021(111):11. https://doi.org/10.1038/s41598-021-81443-w.
[29] Krys P, Matyjaszewski K. Kinetics of Atom Transfer Radical Polymerization. Eur Polym J 2017;89:482–523. https://doi.org/10.1016/J.EURPOLYMJ.2017.02.034.
[30] Liu L, Zhang H, Zhou Y. Quasi-static mechanical response and corresponding analytical model of laminates incorporating with nanoweb interlayers. Compos Struct 2014;111:436–45. https://doi.org/10.1016/J.COMPSTRUCT.2014.01.021.
[31] Obande W, Ó Brádaigh CM, Ray D. Continuous fibre-reinforced thermoplastic acrylic-matrix composites prepared by liquid resin infusion – a review. Compos Part B Eng 2021;215:108771.
[32] Suzuki Y, Cousins D, Wassgren J, Kappes BB, Dorgan J, Stebner AP. Kinetics and temperature evolution during the bulk polymerisation of methyl methacrylate for vacuum-assisted resin transfer molding. Compos Part A Appl Sci Manuf 2018;104:60–7. https://doi.org/10.1016/j.compositesa.2017.10.022.
[33] Madsen B, Thygesen A, Lilholt H. Plant fibre composites–porosity and stiffness. Compos Sci Technol 2007;67:1584–600. https://doi.org/10.1016/j.compscitech.2006.07.009.
[34] Abdullah SIBS, Iannucci L, Greenhalgh ES. On the translaminar fracture toughness of Vectran/epoxy composite material. Compos Struct 2018;202:566–77. https://doi.org/10.1016/J.COMPSTRUCT.2018.03.004.
[35] Greenhalgh ES. Failure analysis and fractography of polymer composites. Cambridge, UK: Woodhead Publishing Ltd.; 2009.
[36] Fischer B, Sarasini F, Tirillò J, Touchard F, Chocinski-Arnault L, Mellier D, et al. Impact damage assessment in biocomposites by micro-CT and innovative air-coupled detection of laser-generated ultrasound. Compos Struct 2019;210:922–31.
[37] Ramakrishnan KR, Corn S, Le Moigne N, Ienny P, Slangen P. Experimental assessment of low velocity impact damage in flax fabrics reinforced biocomposites by coupled high-speed imaging and DIC analysis. Compos Part A Appl Sci Manuf 2021;140:106137. https://doi.org/10.1016/j.compositesa.2020.106137.
[38] Pournoori N, Corrêa Soares G, Orell O, Palola S, Hokka M, Kanerva M. Adiabatic heating and damage onset in a pultruded glass fiber reinforced composite under compressive loading at different strain rates. Int J Impact Eng 2021;147:103728. https://doi.org/10.1016/J.IJIMPENG.2020.103728.
[39] Han N, Baran I, Zanjani JSM, Yuksel O, An LL, Akkerman R. Experimental and computational analysis of the polymerisation overheating in thick glass/Elium® acrylic thermoplastic resin composites. Compos Part B Eng 2020;202:108430. https://doi.org/10.1016/J.COMPOSITESB.2020.108430.